Design of an energy efficient cylindrical roller bearing

Erdem Acar, Evren Emre Üstün, Mehmet Ali Güler, Ahmet Toros & Ozan Müştak

Published online: 21 Sep 2022.

Submit your article to this journal ↗

View related articles ↗

View Crossmark data ↗

Taylor & Francis
Taylor & Francis Group

Check for updates

Design of an energy efficient cylindrical roller bearing

Erdem Acar[a] (iD), Evren Emre Üstün[a] (iD), Mehmet Ali Güler[b] (iD), Ahmet Toros[c], and Ozan Müştak[c] (iD)

[a]Department of Mechanical Engineering, TOBB University of Economics and Technology, Söğütözü, Ankara, Turkey; [b]College of Engineering and Technology, American University of the Middle East, Egaila, Kuwait; [c]R&D Department, Ortadoğu Rulman Sanayi ve Tic. A.Ş., Polatlı, Ankara, Turkey

ABSTRACT

In this study, the roller and ring raceway profiles of a cylindrical roller bearing (CRB) are designed. Starting from an initial design (i.e., an existing CRB, named NJ 309 EP4), it is intended to minimize the friction moment without sacrificing the fatigue life to have an energy efficient roller bearing. The crown heights in the roller profile, and the radius of the raceway camber profile are selected as design variables. Finite element models are developed for friction moment and fatigue life estimation using ANSYS software. Various combinations of the crown height and the radius of the raceway camber profile are evaluated, and the combination leading to minimum friction moment without sacrificing the fatigue life is obtained (i.e., a redesigned CRB is obtained). Friction moment tests and fatigue tests are conducted on the redesigned CRB (named NJ 309 OP). When the test results of the existing and redesigned bearings are compared, it is found that the friction moment of the redesigned bearing is 29% lower than that of the existing bearing, while the L_{10} fatigue life being only 3% smaller. When the test results are evaluated statistically, it is concluded that the difference between the friction moment test results of the existing and redesigned bearings is statistically significant, whereas the difference between the fatigue test results of the existing and redesigned bearings is statistically insignificant.

1. Introduction

Interest in environmentally friendly products, ever-increasing environmental awareness of customers, and laws on emission and waste reduction force bearing manufacturers to use green technologies in product design. To support green technology, bearings should be energy efficient, have minimal environmental impact, and be recyclable.

The cylindrical roller bearings (CRBs) have greater radial load capacity than ball bearings of same external dimensions. These bearings have a high radial load capacity, and are in particular suitable for high speeds and heavy duties. The applications of CRBs include pumps, and compressors, mechanical presses, electric motors, gearboxes, railway vehicles, steelworks and various other industrial applications (Berner et al. 1982; Celin and Kmetič 2008; Yu and Yang 2011; Abdan et al. 2019; Liu and Xu 2022).

For the structural performance of CRBs, the rolling contact problem plays a critical role. The rolling contact problem can be divided into two parts: normal and tangential problems. While

---

the normal solution is related to the normal pressure and the contact patch; the tangential problem is associated with friction and its effects. The surface shear stress distribution depends on the traction force and coefficient of friction. The distribution of surface shear stress is expressed with the slip and stick areas in the contact patch. Slip is the relative velocity between the two material particles that are in contact, and its size in the contact patch changes depending on the value of traction. Hertz (1882) solved the normal problem of contact between quadratic surfaces. For 2D frictional rolling contact problem, Carter (1926) developed his model and handled the surface shear stress in the contact patch. Vermeulen and Johnson (1964) asserted a model for 3D frictional rolling contact by assuming an elliptical contact area. Kalker (1990) solved the 3D frictional rolling contact problem for arbitrary creepages in both lateral and longitudinal directions using several numerical methods. Guler, Alinia, and Adibnazari (2012) developed a 2D analytical solution for the problem, which can be applied to 3D problems with its adaptivity for both plane stress and plane strain geometries.

For complex geometries, the aforementioned analytical approaches are not fully applicable, therefore numerical analysis techniques (e.g., finite element method, FEM) are often used. Demirhan and Kanber (2008) used ANSYS finite element software (ANSYS Inc. 2019) to study the stress and deflection distributions in the bearing's internal and outer races, taking into account the deflection of elastic rings. Ye et al. (2013) explored the effects of tilting misalignment between the inner and outer rings on the distribution of loads on roller bearings using the quasi-dynamic method and the FEM using ANSYS. Lostado, Martinez, and Mac Donald (2015) studied the contact stresses in double-row tapered roller bearings using the finite element method, experimental analysis, and analytical models. Later, Lostado, Escribano García, and Fernandez Martinez (2016) optimized the operating conditions for a double-row tapered roller bearing using a multiple response surface optimization approach. Zhao and Li (2016) proposed an implicit-explicit sequential FE model generated in ANSYS to solve the transient rolling contact problem in wheel-rail interactions, with the consideration of velocity dependent friction. Li et al. (2018) developed a damage-mechanics-based approach using an explicit FE model generated using ABAQUS software to perform cyclic rolling contact stress analysis, in which the roller rolls along the contact surface.

Rolling element bearings are designed for maximum fatigue life, maximum wear life, maximum static load ratio, minimum friction moment, and minimum rotation rate (Hamrock and Anderson 1985; Changsen 1991). Since a flat profile of the rolling element results in the edge stress concentrations at roller ends, Kamamoto, Fujimoto, and Yamamoto (2001) investigated the effect of crowning profile of the cylindrical rollers in CRBs on load carrying capacity. Kumar, Tiwari, and Prasad (2009) obtained optimum design of crowned CRBs to maximize their fatigue life. Cui and He (2015) proposed a new logarithmic profile model of CRB to increase its fatigue life, avoid the edge effect and allow a straight portion on the roller considering uniform pressure distribution and easier manufacturing. Heras, Aguirrebeitia, and Abasolo (2017) proposed a numerical method to calculate the friction torque in a slewing bearing due to manufacturing errors. Halminen et al. (2017) established a multibody model to study the influence of the surface waviness on the friction torque of a touchdown bearing. Xu and Li (2015) studied the influence of the surface waviness on the friction torque of a ball bearing. Liu, Yan, and Shao (2018) proposed an analytical method for calculating the friction torque of a needle roller bearing without and with the roundness error. To the best of the authors' knowledge, there is no study in the literature that takes both fatigue life and friction moment considerations into account. This article aims to fill that gap and presents design of an energy efficient NJ type CRB.

The article is organized as follows. Design of the roller profile and ring raceway profile of the CRB based on friction moment and fatigue life considerations is discussed in Section 2. Details of the FE models developed for friction moment and fatigue life estimation using ANSYS software are given in Section 3. Friction moment tests and fatigue tests conducted on the existing bearing to validate the FE models developed in Section 4. The process of obtaining the redesigned bearing

Table 1. Geometrical properties of NJ309 EP4.

Inner diameter (mm)	45
Outer diameter (mm)	100
Bearing width (mm)	25
Number of rolling elements	13
Diameter of rollers (mm)	15
Roller length (mm)	16

is presented in Section 5. Results of the friction moment and fatigue life tests conducted on the redesigned CRB is provided and evaluated in Section 6. Finally, a summary of important conclusions is given in Section 7.

2. Problem definition

In this study, an NJ type CRB (NJ309 EP4) manufactured by Ortadoğu Rulman Sanayi (ORS) is taken into account. The geometrical properties and CAD model of the bearing are presented in Table 1 and Fig. 1, respectively. The inner and outer raceways as well as the rollers are made from 100Cr6 material, the cage is made from PA66GF25 material (25% glass fiber-reinforced). This bearing is widely used in agricultural implements, tractors and textile machinery, according to the ORS sales reports.

The rollers in CRBs are crowned, since a flat profile of the roller results in the edge stress concentrations at roller ends. In NJ309 EP4 series CRB, the rolling elements have a parabolic crown profile as shown in Fig. 2. At the mid-section of the roller, the crown height is nominal.

In this study, it is intended to minimize the friction moment without sacrificing the fatigue life. As the roller profile plays an important role, the effects of changing the crown profile on friction moment and fatigue life are explored in this study. Various values of the maximum crown height are considered in this study, as shown in Fig. 3.

Another factor that plays an important role is the radius of the raceway camber profile (depicted with R in Fig. 4). The effects of changing the radius of the raceway camber profile on friction moment and fatigue life are also explored in this study.

In summary, the crown heights in the roller profile and radius of the raceway camber profile are selected as design variables. Various combinations of these design variables are considered and the combination that leads to the best performance is selected for further consideration as explained in the subsequent sections.

3. Finite element modeling

In this section, details of the finite element models generated for the friction moment and the fatigue life prediction are presented.

3.1. Finite element model for the friction moment prediction

In the finite element model generated for the friction moment prediction, the CAD model of the entire bearing is utilized as shown in Fig. 5. The bearing geometry is partitioned so that the FE mesh can be generated in a better element quality. The inner and outer rings are divided into 13 (i.e., the number of rollers) equal parts. In the rollers, a similar division is made so that the nodal points on the contact surface can match those on the rings. Since the cage geometry is relatively complex, it is subjected to a more complex partitioning as shown in Fig. 5 to make it suitable for controlling the number of nodes and elements and creating a hexahedral mesh.

To reflect the physical conditions of the problem to the finite element model, various contact and connection definitions are made. A bonded contact is defined between the bearing outer ring
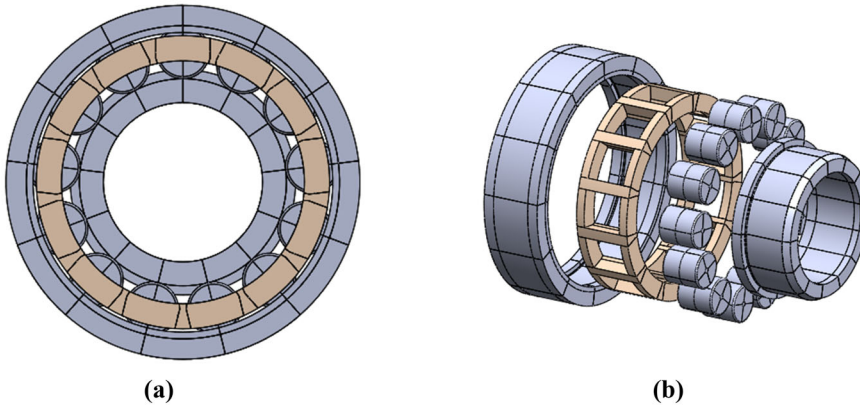
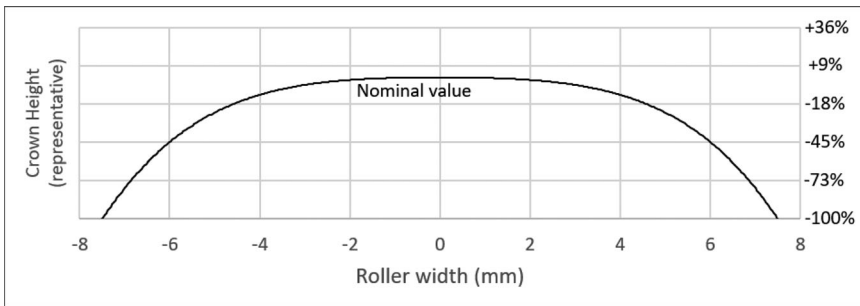**Figure 1.** CAD drawings of NJ309 EP4. (a) Front view, (b) exploded view.

Figure 2. Roller crown profile of the NJ309 EP4 bearing.
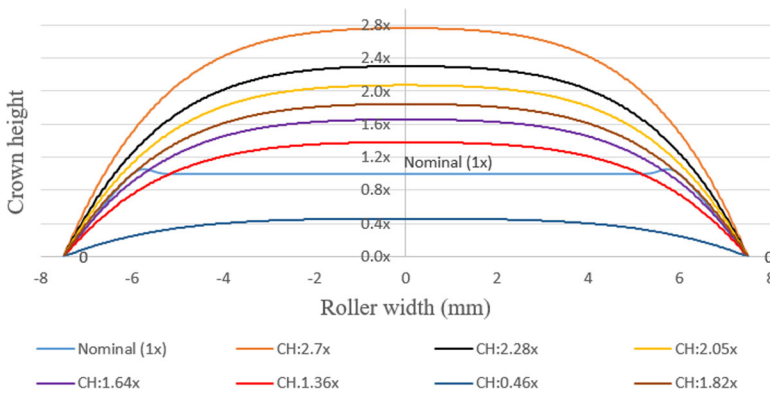

Figure 3. Various values of the maximum crown height.

and the chamber. Thus, an independent movement between the outer ring and the chamber is prevented. In addition, frictional contacts are defined between the roller and ring surfaces. A frictional contact is defined between the roller and the inner ring. Also, frictional contact is defined between the cage and the rollers. The friction coefficients used in these contact definitions are given by the ORS company. Also, more information about the contact definitions are provided in Appendix A.

To define the degrees of freedom of the bodies in the finite element model and to adjust their displacement behavior, various connections are assigned to these bodies. A rotational joint is used to enable the inner ring to rotate around its own axis (see Fig. 6a). Similarly, the outer ring
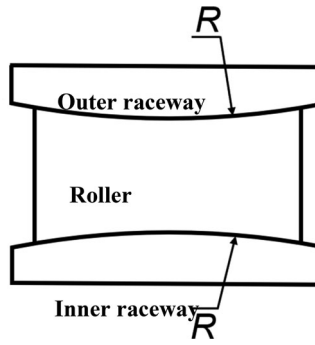
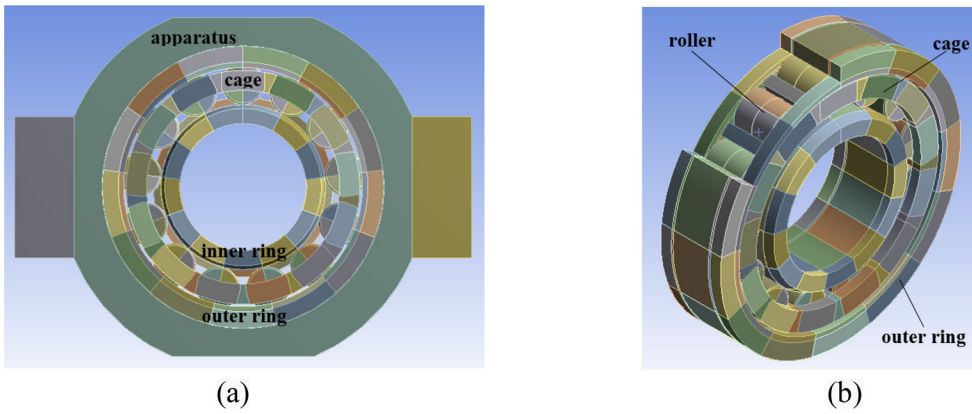**Figure 4.** Schematic depiction of the radius of the raceway camber profile.

(a)

(b)

Figure 5. (a) The front view, (b) isometric view of the CAD model generated for friction moment prediction.
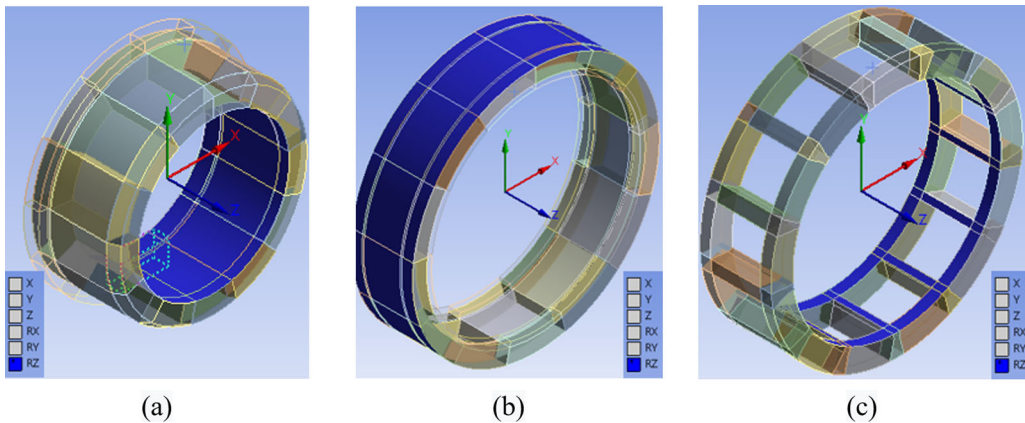

(a)

(b)

(c)

Figure 6. The rotational joints assigned to (a) the inner ring, (b) the outer ring, (c) the cage.

and cage geometry are also adjusted to rotate through the rotational joint assigned to the surfaces indicated in blue in Fig. 6(b,c). In accordance with this connection type, other degrees of freedom of the bodies are limited.

To reflect the displacement behavior of the rollers during the rotation of the bearing, separate planar joints are used for each roller (see Fig. 7). Accordingly, each roller can display vertical and horizontal displacement behavior depending on its reference coordinate system. Besides, due to

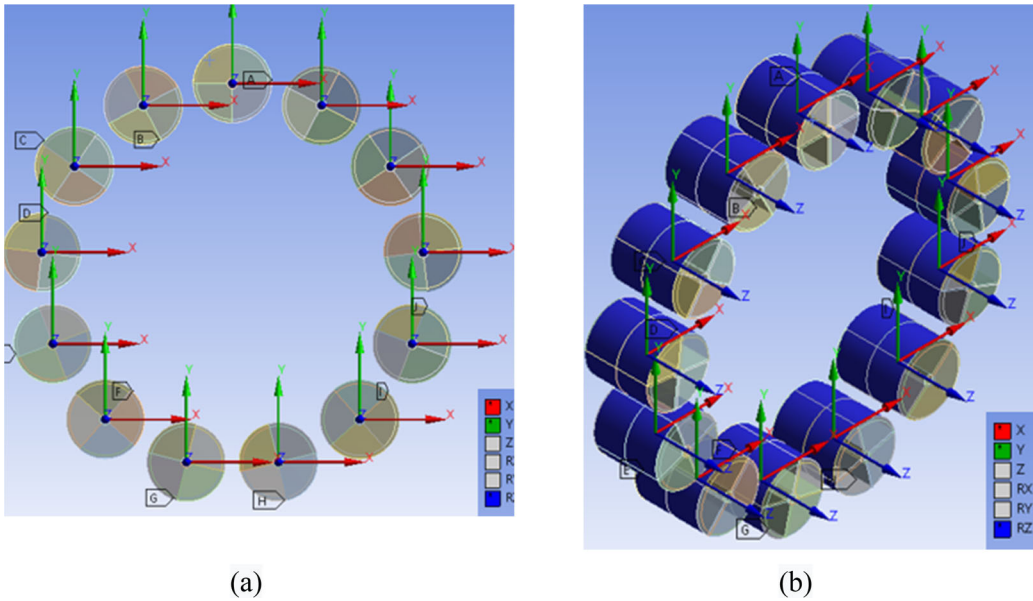(a)   (b)

Figure 7. The planar joints assigned to the rollers. (a) The front view, (b) the isometric view.

its rolling contact behavior, it can rotate around its own rotational axes, whereas the other degrees of freedom are restricted.

The mesh for the FE model developed for friction moment estimation is generated such that it consists mostly of hexagonal elements and the elements are not skewed. In addition, the mesh qualities for all models were checked according to the aspect ratio, Jacobian ratio, warping ratio, and skewness values. For the aspect ratio, the ideal value was 1, while values less than five were considered acceptable. For the Jacobian ratio, the ideal value is 1; however, values greater than 0.5, were considered acceptable. For the warp angle, the ideal value was 0°, with values less than 30° considered acceptable. Finally, for skewness, the ideal value was 0°, with values less than 45° being considered acceptable. ANSYS SOLID186 element type is used in this study. This element type is a higher order 3D 20-node solid element that exhibits quadratic displacement behavior. It supports plasticity, hyperelasticity, creep, stress stiffening, large deflection, and large strain capabilities. It can be used to solve a wide range of problems including 3D contact problems. The partitioning of the geometry (shown earlier in Fig. 5) before creating the mesh was beneficial in improving element quality. The FE mesh generated for the bearing and chamber is shown in Fig. 8. The internal view of the mesh structure formed for the rings and rollers are depicted in Fig. 9. An element size of 1 mm is used in all contact areas in the bearing based on the mesh convergence study results presented in Table 2. Starting from 2 mm mesh size, the element size is progressively reduced in 0.5 mm intervals, and the differences between consecutive friction moment results are computed. The iterations are stopped when the percent difference is less than or equal to 2%.

The friction moment tests are performed under a radial force of 392.4 N Therefore, a force of $F_Y = 196.2$ N is applied to the chamber from both sides as presented in Fig. 10(a). Rotation is applied to the inner ring by means of the defined rotary connection. In the FE model, the chamfer is fixed at locations A and B as shown in Fig. 10(b), and the moment reactions at these locations are determined (see Fig. 11a,b). The sum of these moment reaction provides the friction moment estimation for the bearing.
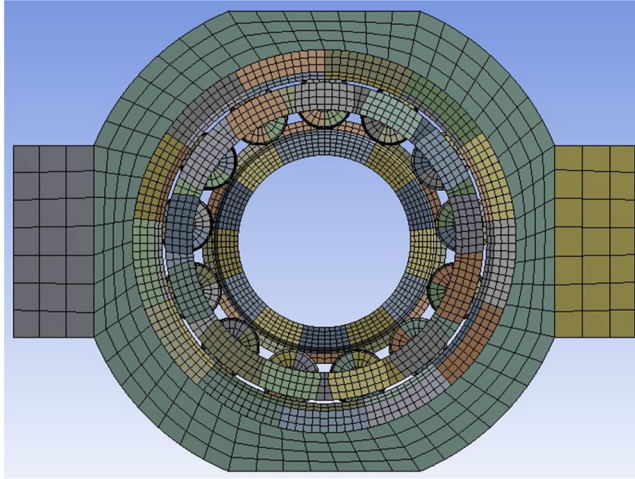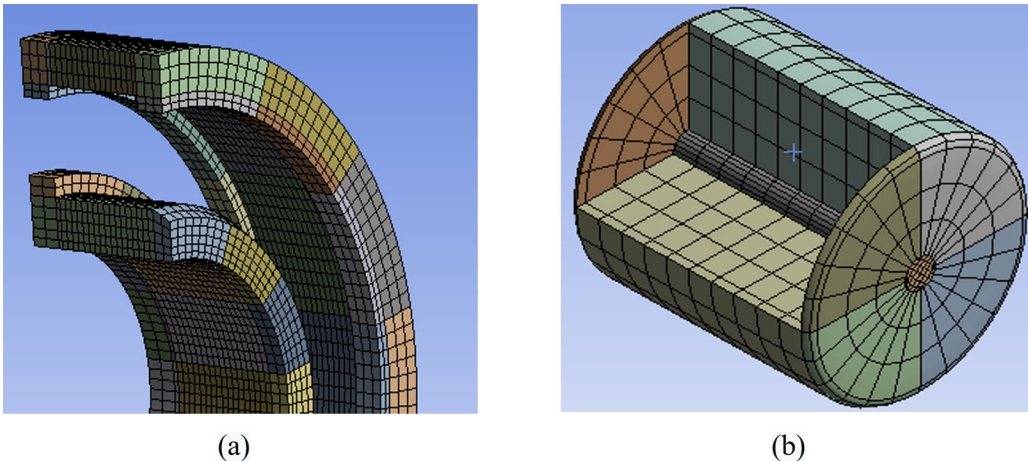
Figure 8. The FE mesh of the bearing and the chamber.

(a)   (b)

Figure 9. Internal view of the mesh structure formed for the rings and rollers.

Table 2. Variation of the friction moment prediction with respect to the element size on the contact surface.

Element size (mm)	Total number of nodes	Solution time	% Difference compared to the best result	% Difference compared to the next result
2.0	122,586	1 h 25 min	10.7	6.2
1.5	163,443	1 h 47 min	4.8	2.9
1.0	243,854	2 h 04 min	2.0	2.0
0.5	431,621	5 h 32 min	–	–

3.2. Finite element model for the fatigue life prediction

Due to the nature of the test conditions of the friction moment estimation, it was not possible to reduce the overall model. For the fatigue life prediction, on the other hand, it is possible to reduce the overall model by concentrating around the roller, which is subjected to the largest load. Note that, the bearing is subject to 31 kN radial load. MESYS software is used to compute the radial load applied on each roller. Table 3 shows that the roller #4 is subjected to the largest radial load of 12.05 kN. In the subsequent analysis, a FE sector model of this particular roller
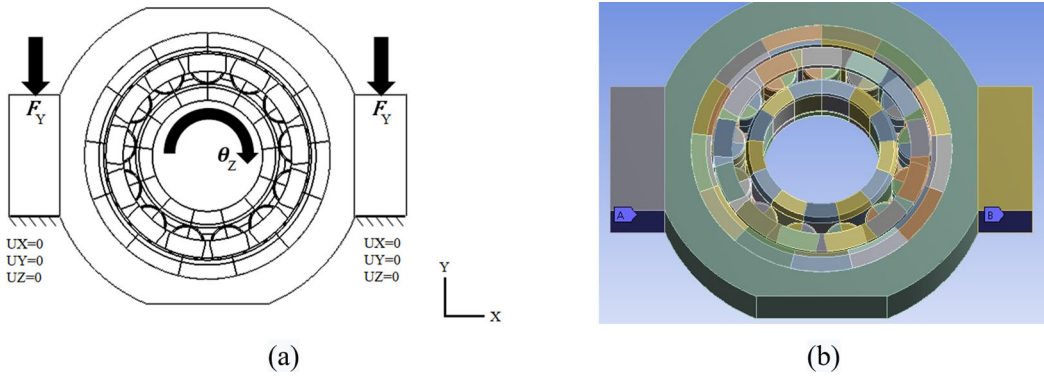
Figure 10. The boundary conditions for the friction moment estimation problem. (a) The test setting, (b) the FE model.
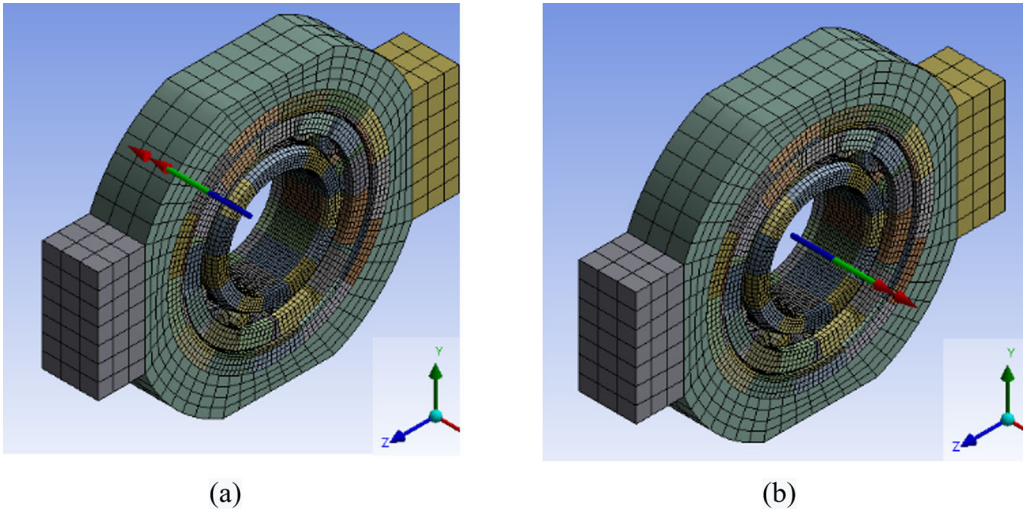

Figure 11. The moment reactions (mesh size of 1 mm is used in the contact regions).

Table 3. Radial loads applied to the rollers.

Roller	Ψ (°)	F_r (kN)	Roller	Ψ (°)	F_r (N)
1	0	0	8	193.8	0
2	27.6	−0.26	9	221.5	0
3	55.3	−6.51	10	249.2	0
4	83.0	12.05	11	276.9	0
5	110.7	−9.74	12	304.6	0
6	138.4	−2.44	13	332.3	0
7	166.1	0	–	–	–

(i.e., 1/13 slice of the full bearing model) is generated, since the contact stresses developed in this region will be higher than the other regions, and the most damage is predicted to occur in this region. The numbering of the rollers is shown in Fig. 12.

Under the test conditions, the force applied on the bearing is delivered by the chamber surrounding the bearing outer ring. Therefore, the chamber is also partitioned in the sectoral modeling (see Fig. 13a). As seen from the side and isometric views shown in Fig. 13(b,c), a more detailed division is made, especially in the roller and the inner ring in an effort to use a finer mesh in the region where the contact takes place.
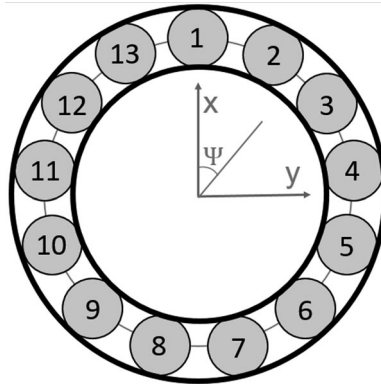
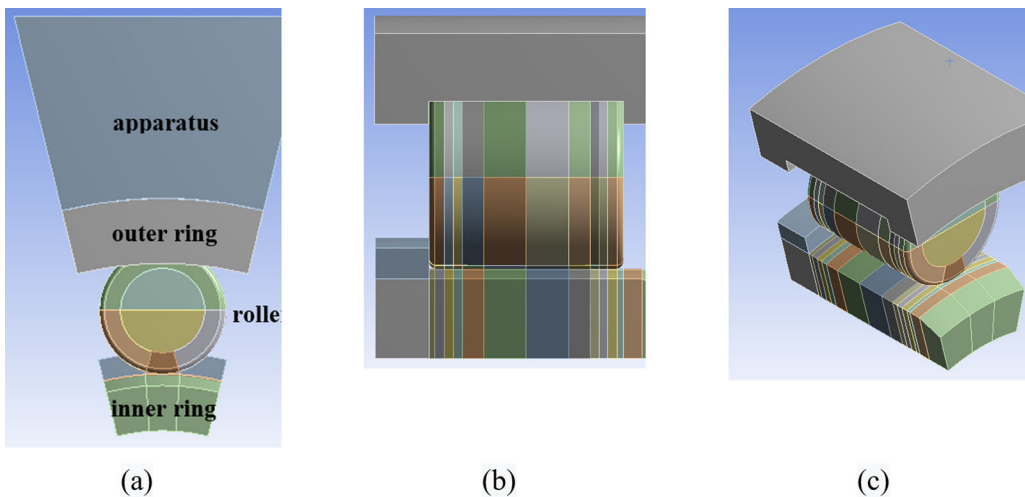**Figure 12.** The numbering of the rollers.

Figure 13. 1/13 sector of the full bearing model. (a) Front view, (b) side view, (c) isometric view.

To reflect the physical conditions of the problem to the finite element model, various contact and connection definitions are made. The first contact definition is between the chamber where the radial force is applied and the outer ring to which the chamber is connected. Taking into account the mounting method in the tests, a bonded contact is defined between the inner surface of the chamber and the outer surface of the outer ring so that the relative movement of the chamber and outer ring is prevented. In addition, frictional contacts are defined between the roller and the ring surfaces. The friction coefficient used in frictional contacts is taken as suggested by the ORS company. More information about the contact definitions are provided in Appendix B.

After the contact definitions, certain connections are assigned to these bodies in order to be able to define the motion of the bodies in the problem geometry. First, a linear connection is assigned to the outer ring, which allows movement only in the vertical direction. This connection, assigned to the outer surface of the outer ring, is controlled by a reference coordinate system shown in Fig. 14(a), and all degrees of freedom are restricted except for movement in the y-direction. A rotation joint is assigned to the inner ring to provide rotation about the rotation axis of the bearing. This connection, shown in Fig. 14(b), allows the inner ring to rotate about the z-axis with respect to the reference coordinate system and restricts other degrees of freedom. Another defined connection is the planar joint assigned to the roller. This connection, shown in
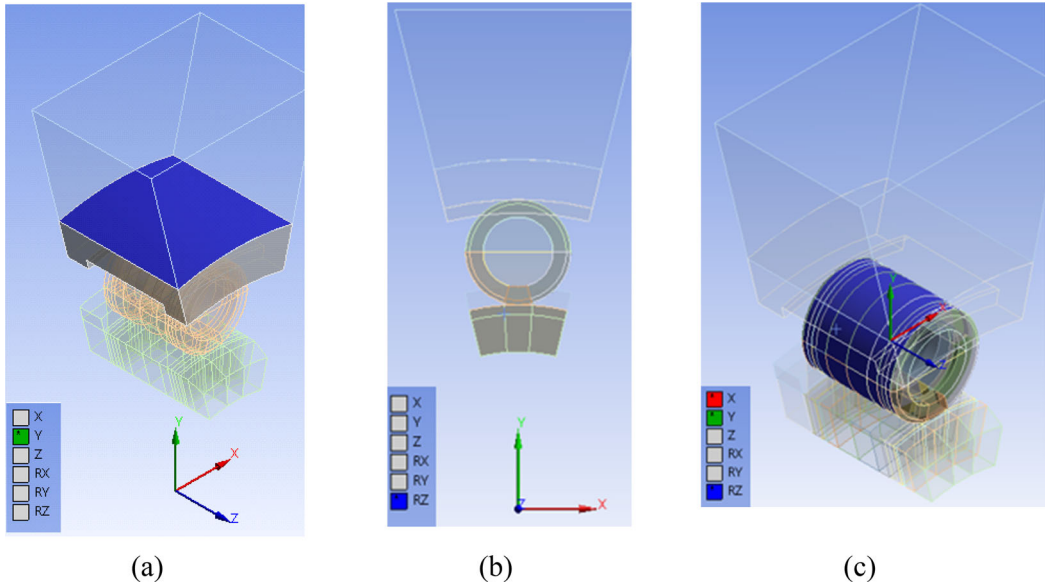
Figure 14. Connections assigned to (a) the outer ring, (b) the inner ring, (c) the roller.

Fig. 14(c), allows the roller to move in vertical and horizontal directions while being able to rotate around its own rotation axis (a requirement of the rolling contact). Other degrees of freedom of the roller are restricted.

To predict the contact stresses correctly, different parts of the FE model are discretized at different mesh densities. A denser mesh structure is preferred in the contact regions and a coarse mesh in the other regions. The mesh of the FE model generated for fatigue life prediction is shown in Fig. 15.

Figure 16 shows a close up view to the roller and the inner ring in the FE model. It is seen that hexagonal elements are preferred and the dimensions of these elements get smaller as they approach the contact area. The aspect ratio approaches to 1:1 for elements in the contact area, this ratio increases with distance from the contact area. Another important point is that the nodal points on the contact surfaces match each other. Matching the nodal points on the roller and ring surfaces is important to have a correct and convergent solution.

A mesh convergence study is performed by gradually reducing the size of the elements on the contact surface. Variation of the maximum contact stress obtained in the model with respect to the element size is monitored, and 0.3 mm element size is found to be suitable as presented in Table 4. Note that the mesh convergence is based on the maximum contact stress, which is then used in fatigue life estimation. Starting from 0.5 mm mesh size, the element size is progressively reduced in 0.1 mm intervals, and the differences between consecutive maximum contact stress results are computed. The iterations are stopped when the percent difference is less than or equal to 1%.

To reflect the test conditions, force must be applied through the chamber to the bearing sector of interest in the model. The force of 12.05 kN, computed earlier using MESYS software and acting on the roller #4, is applied from the upper surface of the chamber as shown in Fig. 17. Rotation condition is applied to the inner ring on the rotating joint defined. Accordingly, the inner ring is subject to an angular velocity of 2000 rpm.

An empirical formula developed in accordance with AISI 52100 material is used to convert the obtained contact stress values into fatigue life values (Raje and Sadeghi 2009). In this formula, which was developed based on the study of Lundberg and Palmgren (1947), the three-parameter Weibull distribution is used instead of the two-parameter Weibull distribution. In this study, in
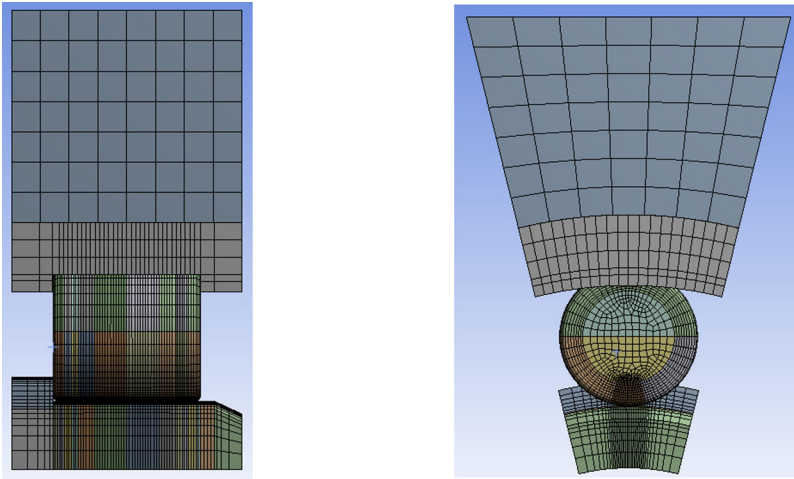
Figure 15. The mesh of the FE model generated for fatigue life prediction. (a) Side view, (b) front view (mesh size of 0.3 mm is used in the contact regions).
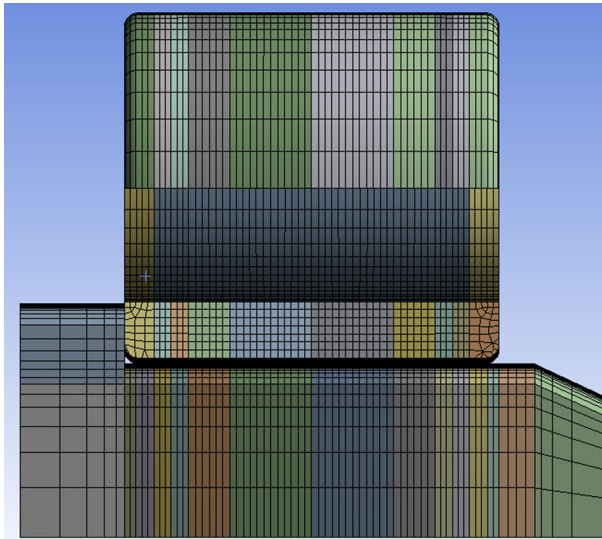

Figure 16. The mesh of the FE model generated for fatigue life estimation in a close up view to the roller and the inner ring.

Table 4. Variation of the maximum contact stress with respect to the element size on the contact surface.

Element size (mm)	Total number of nodes	Solution time	% Difference compared to the best result	% Difference compared to the next result
0.5	120,719	1 h 50 min	5.9	3.9
0.4	167,968	2 h 20 min	2.1	1.9
0.3	296,440	3 h 30 min	0.3	0.3
0.2	496,314	6 h 10 min	–	–

which variables such as contact stresses, geometric parameters, and material properties are taken into account, the use of the three-parameter Weibull distribution provides a significant improvement in the stress-life values due to contact stresses. The maximum contact stresses found as a result of the finite element analysis are converted to cyclic life using Eq. (1).
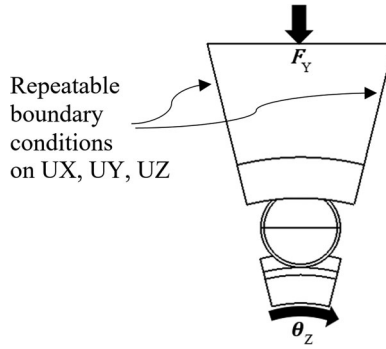
Figure 17. Loading and boundary conditions on the bearing sector.

$$N = \frac{39354}{p_{max}^{8.74}} \left[ln\left(\frac{1}{S}\right) \right]^{0.58}, \tag{1}$$

where N is the number of fatigue cycles (in millions), p_{max} is the maximum contact stresses (in GPa), and S is the reliability (takes as 90% to predict L_{10} life). Using Eq. (1) with $p_{max} =$ 2.032 GPa and $S = 90\%$, the FE model prediction is obtained.

4. Finite element model validation using tests

4.1. Validation of the FE model for friction moment prediction

To validate the FE model for friction moment prediction, friction moment tests are conducted using the test machine shown in Fig. 18. The difference between the mean value obtained in the tests and the FE model prediction was found to be 14% higher (FE model prediction) and convergence was achieved. Also, the mean absolute relative error between the test results and the FE model prediction is computed to be 16.6%.

4.2. Validation of the FE model for fatigue life prediction

To validate the FE model for fatigue life prediction, fatigue tests are conducted using the test machine shown in Fig. 19. The bearings are loaded with a radial load of 31 kN applied while the shaft is rotating at 2000 rpm, and tests are conducted for seven different bearings. The fatigue life prediction through FE model is found to be acceptable with difference 28% higher (FE model prediction) considering the high scatter of life values. Also, the mean absolute relative error between the test results and the FE model prediction is computed to be 37.3%.

5. Redesign of the bearing

The crown heights in the roller profile and the radius of the raceway camber profile are selected as the design variables. In redesign of the bearing, the goal was to reduce the friction moment at least 8% without jeopardizing the fatigue life much. That is, it is aimed that the friction moment is at least 8% less than the baseline design without reducing the fatigue life much. Notice that these friction moment and fatigue life values correspond to the FE model predictions rather than experimental values as the subsequent investigations are performed using FE simulations.

On the baseline design, taking into account the maximum crown height (MCH) in the roller profile and the radius of the raceway camber profile (RCP), first, the MCH is varied between no crown (0) and value which is 2.72x higher value than baseline design value (taking values of no
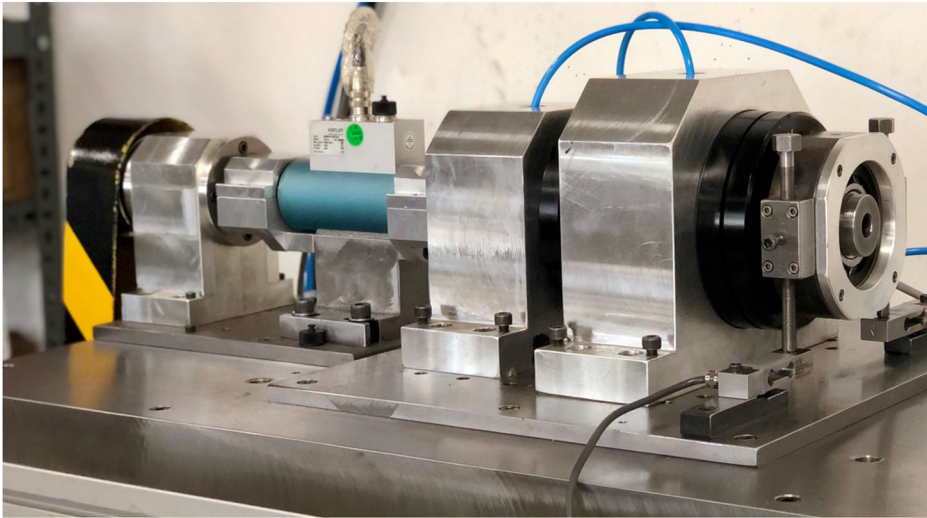
(a)
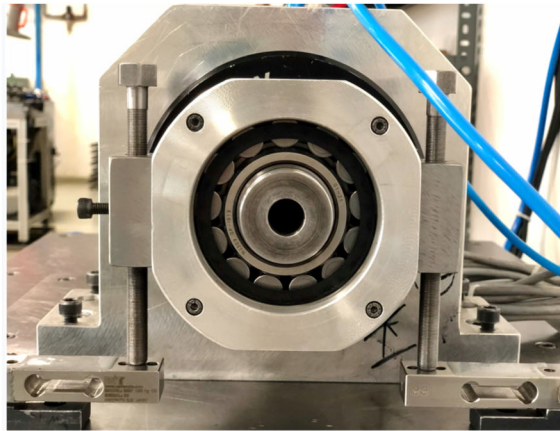
(b)

Figure 18. (a) Isometric and (b) side views of the friction moment test machine.

crown (0), 0.46x, 1x, 1.36x, 1.64x, 1.82x, 2.05x, 2.28x, and 2.72x), while maintaining the keeping the RCP (baseline design value) value steady, and the variations of the friction moment and the fatigue life are monitored (x: baseline design value). Figure 20 shows that the friction moment is 8% (success criterion) smaller than the baseline design value for MCH values of 1.64x, 1.82x, 2.05x. Therefore, these MCH values are selected for further investigation. Figure 21 shows that is smaller than the fatigue life which is obtained from baseline design with FE model for all MCH values larger than the nominal MCH on the baseline design, including the selected MCH values of 1.64x, 1.82x, 2.05x. It is aimed to improve the fatigue life by tailoring the RCP value.

Next, the RCP values is varied between baseline design value and 2.74z value higher than the baseline design value (taking values of z (nominal value for baseline design), 1.37z, 1.65z, 1.92z, 2.20z, 2.47z, and 2.74z), and the variations of the friction moment and the fatigue life are monitored for MCH values of 1.64x, 1.82x, 2.05x (x: nominal value for baseline design). Figure 22
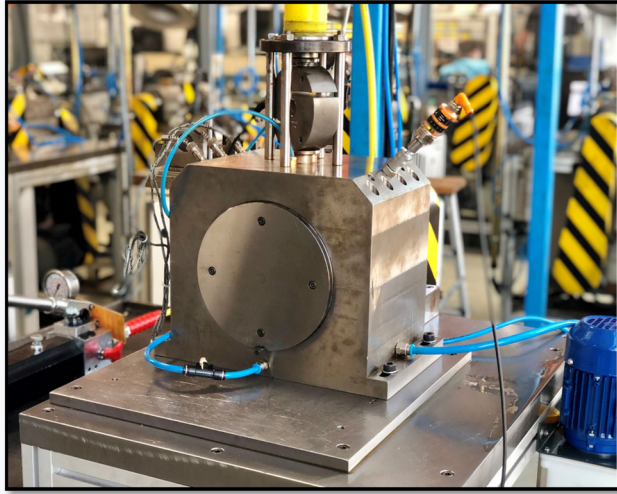
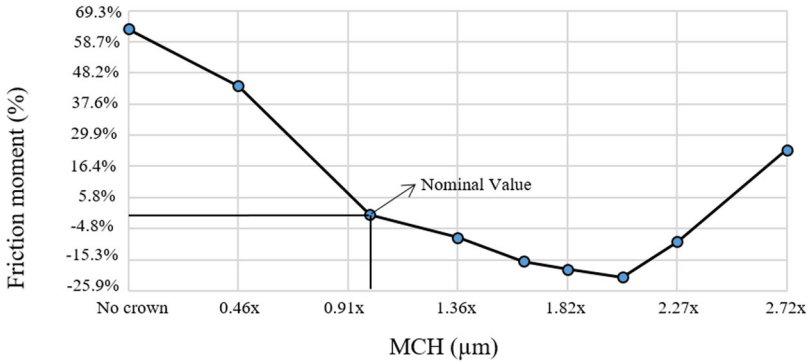**Figure 19.** Isometric view of the fatigue life test machine.

Figure 20. Variation of the friction moment with respect to the maximum crown height, MCH (RCP = this value is kept constant).
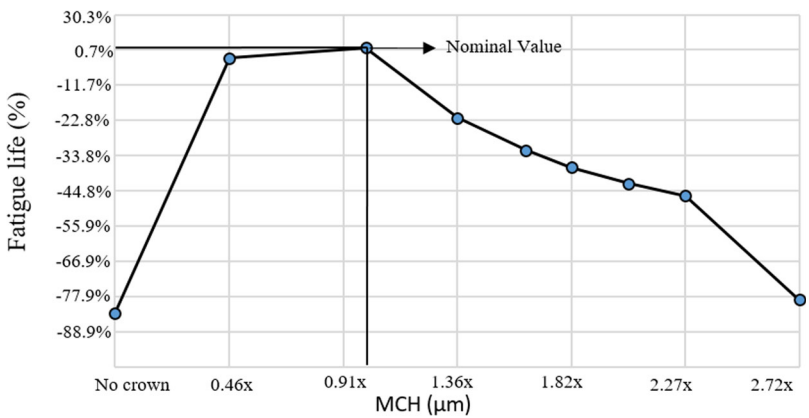

Figure 21. Variation of the fatigue life with respect to the maximum crown height, MCH (RCP = this value is kept constant).

shows that the fatigue file increases as RCP increases, in line with our expectations. On the other hand, Fig. 23 shows that the friction moment also increases as RCP increases. Therefore, a further study is performed for various combinations of MCH and RCP combinations to attain a friction
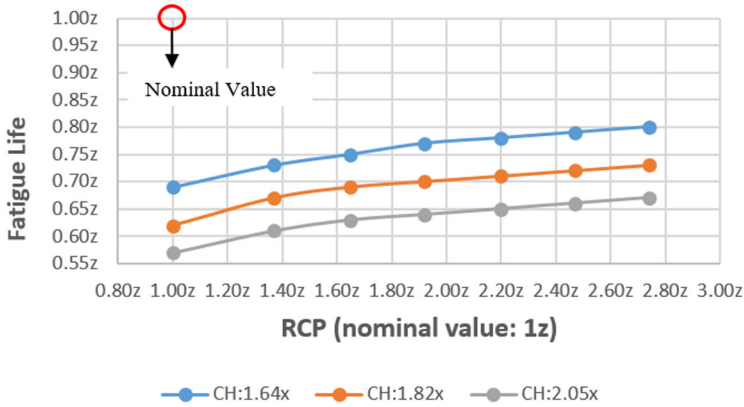
Figure 22. Variation of the fatigue life with respect to the radius of the raceway camber profile, RCP (for CHR values of 1.63*x*, 1.82*x*, and 2.05*x*).
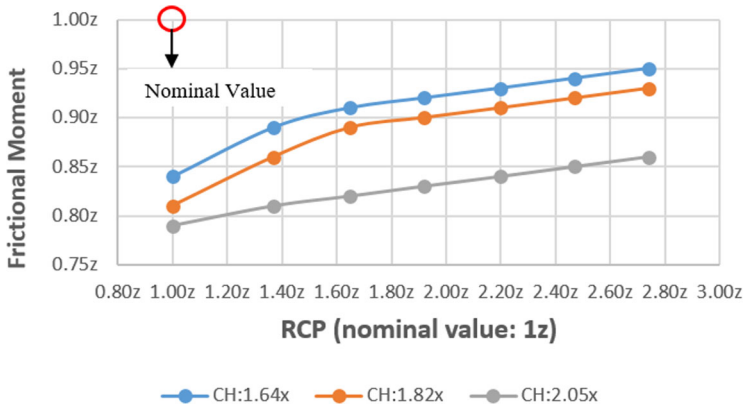

Figure 23: Variation of the friction moment with respect to the radius of the raceway camber profile, RCP (for CHR values of 1.63*x*, 1.82*x*, and 2.05*x*).

moment value that is at least 8% lower than the baseline design without reducing the fatigue life much.

Finally, a tradeoff study is performed next by exploring various combinations of MCH and RCP combinations. For each MCH value determined (that is, 1.64*x*, 1.82*x*, 2.05*x*), a proper RCP value is determined from Figs. 22 and 23, and the corresponding friction moment and fatigue life values are predicted for these design configurations. Table 5 shows that the friction moment is the smallest for MCH = 2.05*x* and RCP = 2.74*z* configuration, whereas the fatigue life is also the smallest. For MCH = 1.64*x* and RCP = 1.65*z* configuration, on the other hand, the fatigue life is the largest, whereas the friction moment is also the largest. The other configuration, MCH = 1.82*x* and RCP = 2.20*z*, has smaller friction moment and slightly smaller fatigue life than MCH = 1.64*x* and RCP = 1.65*z* configuration; hence, MCH = 1.82*x* and RCP = 2.20*z* configuration is decided to be used in the redesigned bearing.

6. Tests results for the redesigned bearing

The friction moment and fatigue life of the redesigned bearing are assessed with tests under the same testing conditions detailed earlier in Section 4. The test results of the redesigned bearing are presented, and compared to those of the baseline design in the subsequent sections.

Table 5. Friction moment and fatigue life values for different design configurations (x: nominal MCH and z: nominal RCP for baseline design).

MCH–RCP combination	Friction moment (N mm)	Fatigue life (h)
MCH $= 1.64x$, RCP $= 1.65z$	1% less	24% less
MCH $= 1.82x$, RCP $= 2.20z$	1.5% less	28% less
MCH $= 2.05x$, RCP $= 2.74z$	6.5% less	33% less
Desired values	8% less than baseline design	As much as possible

6.1. Friction moment tests

Similar to the baseline bearing test, friction moment tests are conducted for seven different bearings. The average value obtained in the tests of the redesigned bearing is 29.1% smaller than that of the baseline bearing.

The friction moment test results obtained for the baseline and redesigned bearings are also compared using t-tests. The probability associated with student's independent t-test, using two-tailed distributions with unequal variances, is computed as 1.04×10^{-5}. This value is substantially smaller than 5%, indicating a statistically significant difference between the average friction moment values corresponding to the redesigned and baseline bearings

6.2. Fatigue tests

Fatigue life tests are conducted for seven different samples of the redesigned bearing. The L_{10} fatigue life obtained in the tests of the redesigned bearing is only 3% smaller than that of the baseline bearing.

The friction moment test results obtained for the baseline and redesigned bearings are also compared using t-tests. The probability associated with student's independent t-test, using two-tailed distributions with unequal variances, is computed as 0.816. This value is substantially larger than 5%, indicating that the difference between the average fatigue values corresponding to the redesigned and baseline bearings is statistically insignificant.

7. Concluding remarks

In this study, the roller and ring raceway profiles of a CRB were designed to minimize the friction moment without sacrificing the fatigue life. FE models were generated for friction moment and fatigue life predictions, and validated with tests. The crown heights in the roller profile, and the radius of the raceway camber profile were selected as design variables. Various combinations of the crown height and the radius of the raceway camber profile were evaluated using the FE models, and a redesigned CRB was obtained. From the results obtained in this study, the following conclusions were drawn:

- The difference between the mean value obtained in the tests and the FE model prediction was found to be 14% and convergence was achieved.
- Similarly, for the baseline bearing, the FE model for fatigue life prediction provided acceptable with a 28% difference compared to the average value obtained in the tests, considering the high scattering of test life values.
- The crown heights in the roller profile, and the radius of the raceway camber profile were selected as design variables. Various combinations of the crown height and the radius of the raceway camber profile were evaluated, and a redesigned CRB was obtained. It was found that the friction moment of the redesigned bearing is 29% lower than that of the existing bearing, while the L_{10} fatigue life being only 3% smaller.

- When the test results were evaluated statistically, it was concluded that the difference between the friction moment test results of the existing and redesigned bearings was statistically significant, whereas the difference between the fatigue test results of the existing and redesigned bearings was statistically insignificant.

Author contributions

E. Acar: Conceptualization, methodology, writing – review and editing, supervision. **E. E. Üstün:** Conceptualization, methodology, formal analysis, investigation, visualization, and writing – original draft. **M. A. Güler:** Conceptualization, methodology, writing – review and editing, supervision. **A. Toros:** Conceptualization, methodology, formal analysis, investigation, visualization. **O. Müştak:** Conceptualization, methodology, writing – review and editing.

Disclosure statement

No potential conflict of interest was reported by the author(s).

Funding

ORCID

Erdem Acar 🆔 http://orcid.org/0000-0002-3661-5563
Evren Emre Üstün 🆔 http://orcid.org/0000-0003-1618-3609
Mehmet Ali Güler 🆔 http://orcid.org/0000-0002-1159-556X
Ozan Müştak 🆔 http://orcid.org/0000-0001-8859-3872

References

Abdan, S., N. Stosic, A. Kovacevic, I. Smith, and N. Asati. 2019. Analysis of rolling bearing power loss models for twin screw oil injected compressor. *IOP Conference Series: Materials Science and Engineering* 604 (1):012013. doi:10.1088/1757-899X/604/1/012013.

ANSYS Inc. 2019. *ANSYS mechanical APDL structural analysis guide.* (ANSYS Version 19). Canonsburg, PA: ANSYS Inc.

Berner, F., H. Oesch, K. Goetz, and C. J. Savage. 1982. The mechanical design of a vapor compressor for a heat pump to be used in space. Paper presented at *16th Aerospace Mech. Symp. in NASA Kennedy Space Center*, 329–40.

Carter, F. W. 1926. On the action of a locomotive driving wheel. *Proceedings of the Royal Society of London A* 112: 151–57.

Celin, R., and D. Kmetič. 2008. Cracks in a roller-bearing. *Metalurgija* 47 (1):69–72.

Changsen, W. 1991. *Analysis of rolling element bearings.* London: Mechanical Engineering Publications Ltd.

Cui, L., and Y. He. 2015. A new logarithmic profile model and optimization design of cylindrical roller bearing. *Industrial Lubrication and Tribology* 67 (5):498–508. doi:10.1108/ILT-01-2015-0006.

Demirhan, N., and B. Kanber. 2008. Stress and displacement distributions on cylindrical roller bearing rings using FEM. *Mechanics Based Design of Structures and Machines* 36 (1):86–102. doi:10.1080/15397730701842537.

Guler, M. A., Y. Alinia, and S. Adibnazari. 2012. On the rolling contact problem of two elastic solids with graded coatings. *International Journal of Mechanical Sciences* 64 (1):62–81. doi:10.1016/j.ijmecsci.2012.08.001.

Halminen, O., J. F. Aceituno, J. L. Escalona, J. Sopanen, and A. Mikkola. 2017. A touchdown bearing with surface waviness: Friction loss analysis. *Mechanism and Machine Theory*. 110:73–84. doi:10.1016/j.mechmachtheory. 2017.01.002.

Hamrock, B. J., and W. J. Anderson. 1985. Rolling element bearings. In *Mechanical design and systems handbook*, ed. H. A. Rothbart. New York, NY: McGraw Hill.

Heras, I., J. Aguirrebeitia, and M. Abasolo. 2017. Friction torque in four contact point slewing bearings: Effect of manufacturing errors and ring stiffness. *Mechanism and Machine Theory*. 112:145–54. doi:10.1016/j.mechmach-theory.2017.02.009.

Hertz, H. 1882. Über die berührung fester elastischer körper. *Journal für die Reine und Angewandte Mathematik* 92:156–71.

Kalker, J. J. 1990. *Three-dimensional elastic bodies in rolling contact*, 137–84. Dordrecht: Kluwer Academic Publishers.

Kamamoto, S., K. Fujimoto, and T. Yamamoto. 2001. Research on crowning profile to obtain the maximum load carrying capacity for roller bearings. *KOYO Engineering Journal* 159E:47–52.

Kumar, K. S., R. Tiwari, and P. Prasad. 2009. An optimum design of crowned cylindrical roller bearings using genetic algorithms. *Journal of Mechanical Design* 131 (5):051011. doi:10.1115/1.3116344.

Li, F., W. Hu, Q. Meng, Z. Zhan, and F. Shen. 2018. A new damage-mechanics-based model for rolling contact fatigue analysis of cylindrical roller bearing. *Tribology International* 120:105–14. doi:10.1016/j.triboint.2017.12.001.

Liu, J., and Z. Xu. 2022. A simulation investigation of lubricating characteristics for a cylindrical roller bearing of a high-power gearbox. *Tribology International* 167:107373. doi:10.1016/j.triboint.2021.107373.

Liu, J., Z. Yan, and Y. Shao. 2018. An investigation for the friction torque of a needle roller bearing with the roundness error. *Mechanism and Machine Theory* 121:259–72. doi:10.1016/j.mechmachtheory.2017.10.028.

Lostado, R., R. Escribano García, and R. Fernandez Martinez. 2016. Optimization of operating conditions for a double-row tapered roller bearing. *International Journal of Mechanics and Materials in Design* 12 (3):353–73. doi:10.1007/s10999-015-9311-4.

Lostado, R., R. F. Martinez, and B. J. Mac Donald. 2015. Determination of the contact stresses in double-row tapered roller bearings using the finite element method, experimental analysis and analytical models. *Journal of Mechanical Science and Technology* 29 (11):4645–56. doi:10.1007/s12206-015-1010-4.

Lundberg, G., and A. Palmgren. 1947. Dynamic capacity of rolling bearings. *Acta Polytechnica. Mechanical Engineering Series* 1 (3):1–52.

Raje, N., and F. Sadeghi. 2009. Statistical numerical modelling of sub-surface initiated spalling in bearing contacts. *Proceedings of the Institution of Mechanical Engineers, Part J: Journal of Engineering Tribology* 223 (6):849–58. doi:10.1243/13506501JET481.

Vermeulen, P. J., and K. L. Johnson. 1964. Contact of non-spherical bodies transmitting tangential forces. *Journal of Applied Mechanics* 31 (2):338–40. doi:10.1115/1.3629610.

Xu, L. X., and Y. G. Li. 2015. Modeling of a deep-groove ball bearing with waviness defects in planar multibody system. *Multibody System Dynamics* 33 (3):229–58. doi:10.1007/s11044-014-9413-z.

Ye, Z., L. Wang, L. Gu, and C. Zhang. 2013. Effects of tilted misalignment on loading characteristics of cylindrical roller bearings. *Mechanism and Machine Theory* 69:153–67. doi:10.1016/j.mechmachtheory.2013.05.006.

Yu, Z. Q., and Z. G. Yang. 2011. Fatigue failure analysis of a grease-lubricated roller bearing from an electric motor. *Journal of Failure Analysis and Prevention* 11 (2):158–66. doi:10.1007/s11668-010-9422-z.

Zhao, X., and Z. Li. 2016. A solution of transient rolling contact with velocity dependent friction by the explicit finite element method. *Engineering Computations* 33 (4):1033–50. doi:10.1108/EC-09-2014-0180.

# Appendix A: Contact definition details for the FE model generated for friction moment prediction

The first definition of contact made is the bonded contact relationship between the bearing outer ring and the chamber (see Fig. A1). Thus, an independent movement between the outer ring and the chamber is prevented.

In addition, frictional contacts are defined between the roller and ring surfaces. The frictional contact defined between the roller and the inner ring is shown in Fig. A2(a). This contact definition, shown here for a single roller, is applied in the same way for the other rollers. The surfaces indicated in red are knitted with CONTA174 elements, and the surfaces indicated in blue are knitted with TARGE170 elements. The friction contact defined between the rollers and the outer ring is shown in Fig. A2(b). Augmented Lagrange contact formulation is used to create the contact definitions in the contact regions. The augmented Lagrangian formulation can accurately detect discontinuities in the contact zone and stabilize the stiffness matrix at each iteration throughout the solution process, therefore this contact formulation is chosen for this study.

The last contact group defined is the contact between the cage and the rollers. Since the cage inner slots and the bobbin outer surfaces are in contact, CONTA174 elements are placed on the bobbin surface, while TARGE170 elements are used for the cage surfaces (see Fig. A3).
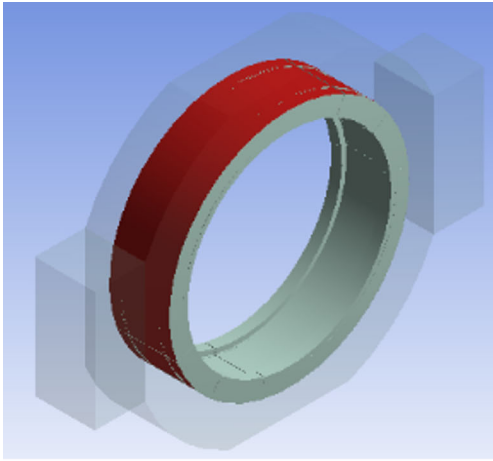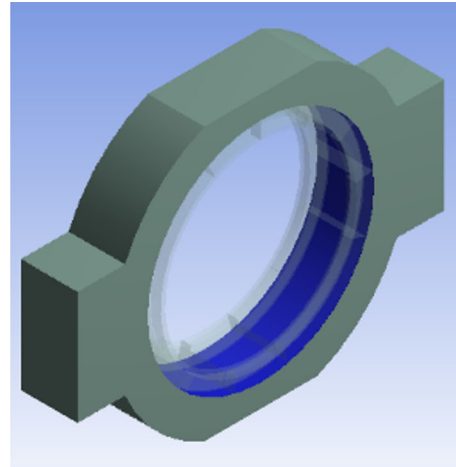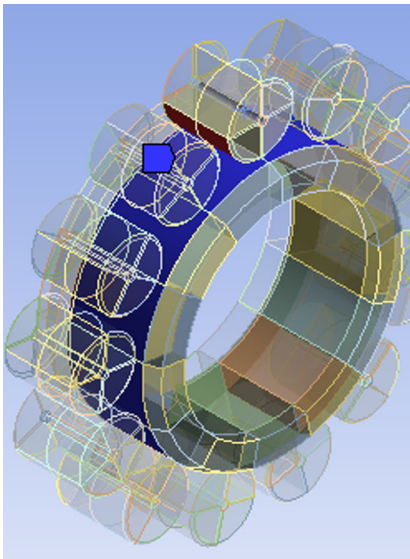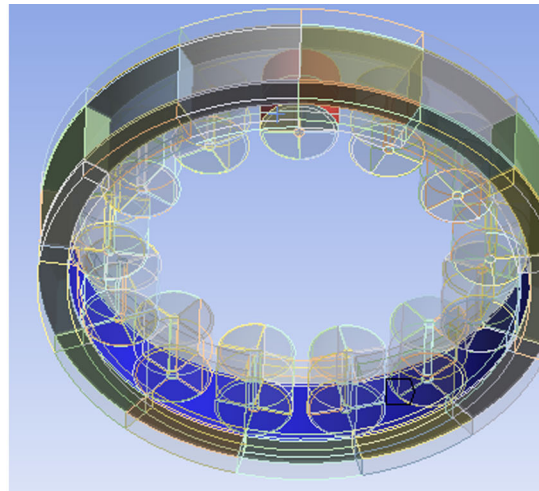
(a)   (b)

Figure A1. The contact defined between the outer ring and the chamber. (a) The outer ring contact surface, (b) the chamber contact surface.

(a)   (b)

Figure A2. Frictional contacts defined between the rollers and the rings. (a) The roller and the inner ring, (b) the roller and the outer ring.
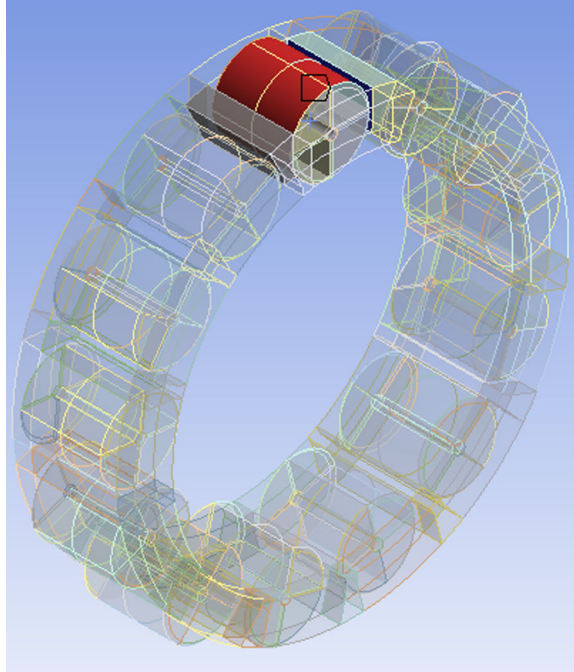
Figure A3. Frictional contact defined between bobbin and cage.

Appendix B: Contact definition details for the FE model generated for fatigue life prediction

In the FE model generated for fatigue life estimation, three contact definitions are made. The first of these is between the chamber where the radial force is applied and the outer ring to which the chamber is connected. Taking into account the mounting method in the tests, a bonded contact was defined between the inner surface of the chamber and the outer surface of the outer ring (see Fig. B1). Thus, relative movement of the chamber and outer ring is prevented.

In addition, frictional contacts are defined between the roller and the ring surfaces. The first of these is the contact of the bobbin with the inner ring; the other involves contact with the outer ring (see Fig. B2). Here, the surfaces shown in red are knitted from the CONTA174 elements, and the surfaces shown in blue are knitted from the TARGE170 elements. The visuals of the frictional contact defined between the bobbin and the outer ring are given in Fig. B3. The friction coefficient used in frictional contacts is given by ORS company.
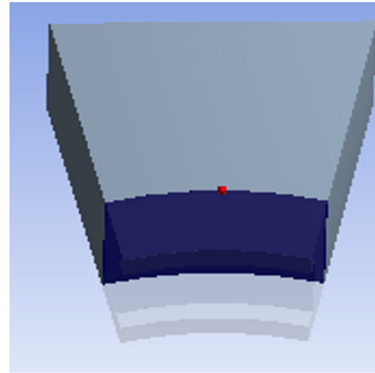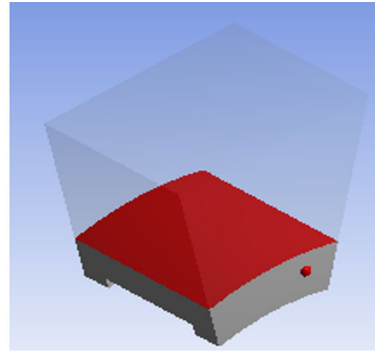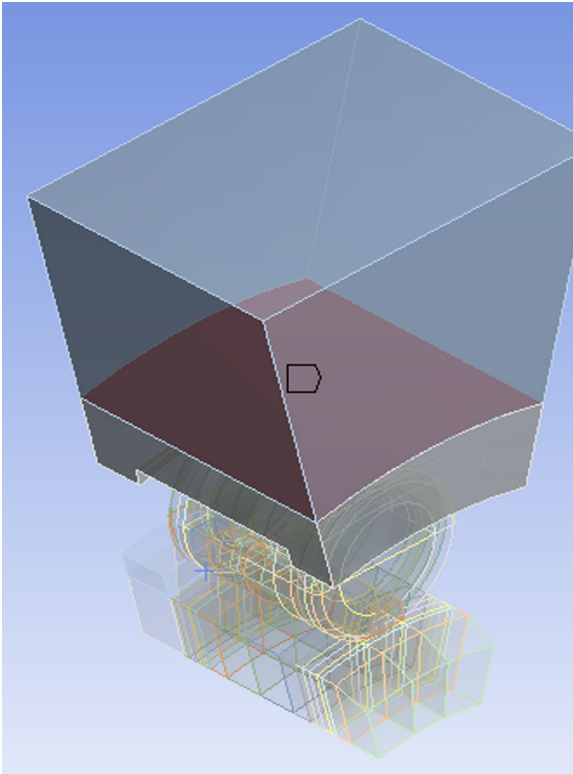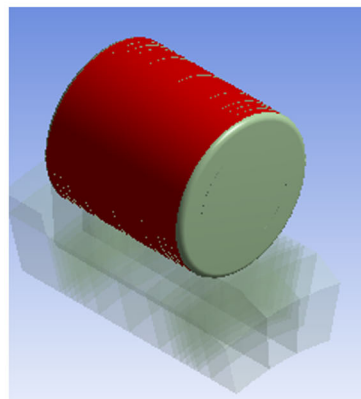
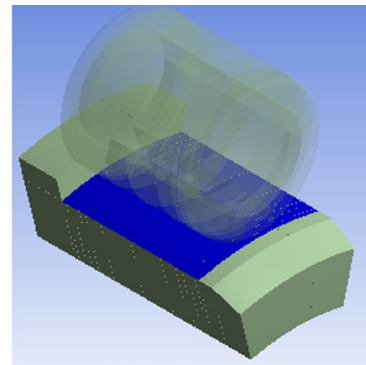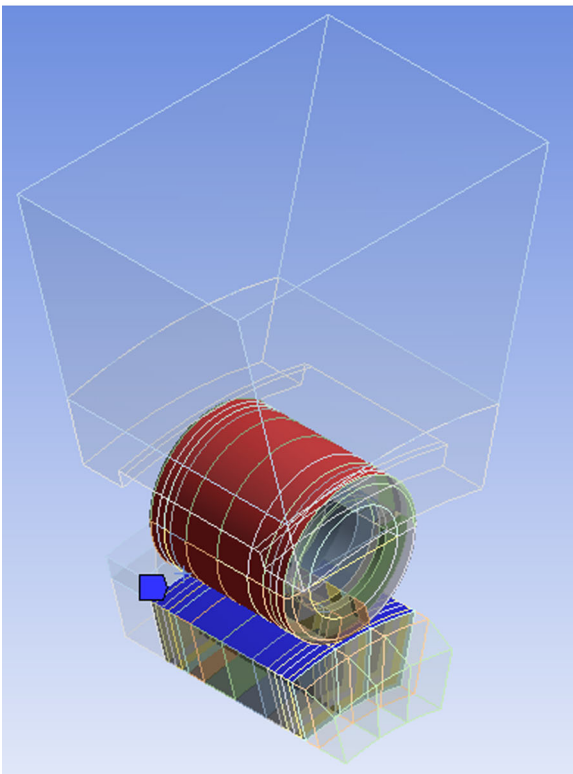**Figure B1.** Contact areas between chamber and outer ring.

Figure B2. Frictional contact areas between the roller and the inner ring.
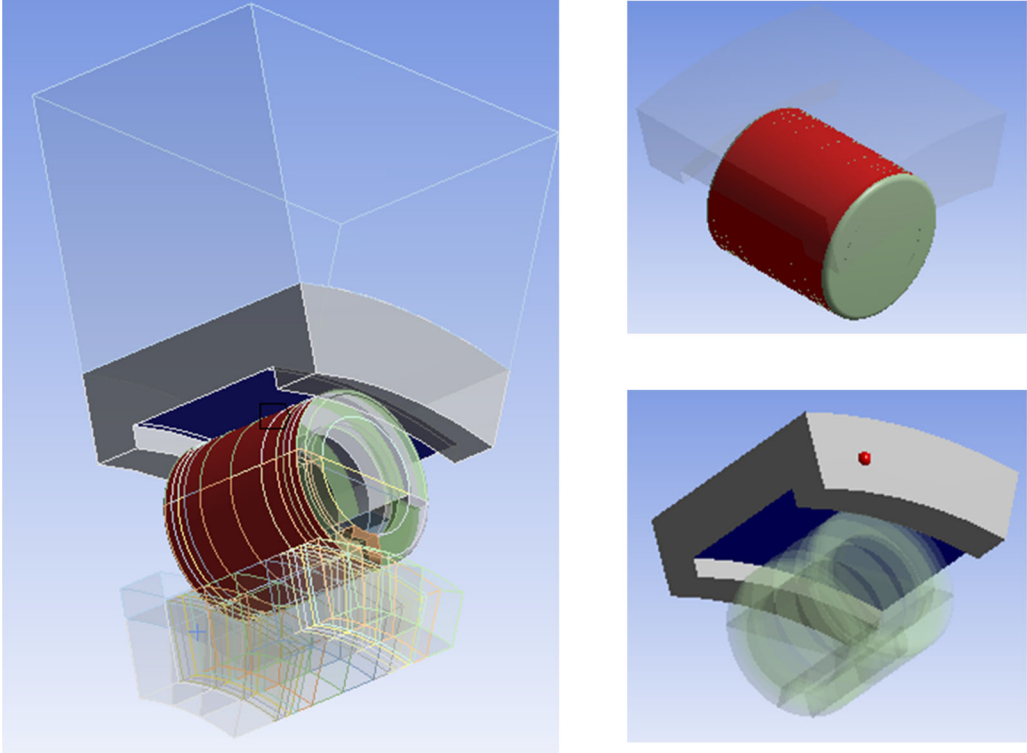
Figure B3. Frictional contact areas between the roller and the inner ring.